Zoology 134 (2019) 16–26

Contents lists available at ScienceDirect

Zoology

journal homepage: www.elsevier.com/locate/zool

Angles and waves: intervertebral joint angles and axial kinematics of limbed lizards, limbless lizards, and snakes

Gen Morinaga*,[1], Philip J. Bergmann

Department of Biology, Clark University, 950 Main Street, Worcester, Massachusetts 01610, USA

ARTICLE INFO

Keywords:
body elongation
axial kinematics
limbless locomotion

ABSTRACT

Segmentation gives rise to the anterior-posterior axis in many animals, and in vertebrates this axis comprises serially arranged vertebrae. Modifications to the vertebral column abound, and a recurring, but functionally understudied, change is the elongation of the body through the addition and/or elongation of vertebrae. Here, we compared the vertebral and axial kinematics of the robustly limbed Fire skink (*Riopa fernandi*) representing the ancestral form, the limbless European glass lizard (*Ophisaurus apodus*), and the Northern water snake (*Nerodia sipedon*). We induced these animals to traverse through channels and peg arrays of varied widths and densities, respectively, using high-speed X-ray and light video. We found that even though the snake had substantially more and shorter vertebrae than either lizard, intervertebral joint angles did not differ between species in most treatment levels. All three species decreased the amplitude and wavelength of their undulations as channels narrowed and the lizard species increased wave frequency in narrower channels. In peg arrays, both lizard species decreased wave amplitude, while the snake showed no differences. All three species maintained similar wavelengths and frequencies as peg density increased in most cases. Our results suggest that amplitude is decoupled from wavelength and frequency in all three focal taxa. The combination of musculoskeletal differences and the decoupling of axial kinematic traits likely facilitates the formation of different undulatory waves, thereby allowing limbless species to adopt different modes of locomotion.

1. Introduction

Segmentation of the anterior-posterior axis is a key feature of many animal phyla and has resulted in the evolution of great morphological and functional diversity (Minelli and Fusco, 2004; Tautz, 2004). Vertebrates are defined by this segmentation, which is manifested as the vertebral column. The vertebral column comprises serially arranged vertebrae that allow the body to flex at their joints (Lauder, 1980; Ward and Mehta, 2014). Vertebral column morphology varies widely among clades (Ward and Brainerd, 2007; Bergmann and Irschick, 2012; Ward and Mehta, 2014), which may affect the flexibility of the vertebral column thereby also affect locomotor kinematics and function, or locomotor strategies (Zug, 1972; Lauder, 1980; Long et al., 1997; Buchholtz, 2001; Bergmann and Irschick, 2010). These changes in locomotor strategies may influence niche use and ecology. For example, increases in vertebral number in the body and tail are thought to facilitate fossorial locomotion and locomotion through structurally-complex habitats, respectively in fishes, lizards, and snakes (Gans, 1974, 1975; Wiens et al., 2006; Brandley et al., 2008; Mehta et al., 2010). Conversely, decreases in anterior vertebral flexibility in chameleons are thought to facilitate an arboreal habit (Fischer et al., 2010). For many vertebrates, limbs generate the propulsive forces for locomotion. However, many clades including some fishes (Mehta et al., 2010; Ward and Mehta, 2010), amphibians (Summers and O'Reilly, 1997; Parra-Olea and Wake, 2001), squamates (Wiens et al., 2006; Brandley et al., 2008), and mammals (Gliwicz, 1988; Buchholtz, 2001) have independently evolved elongated bodies with reduced or absent limbs, leading to a dependence on axial flexion for locomotion (Gans, 1962, 1974, 1975).

These elongate, limb-reduced body shapes can be achieved through the addition and/or elongation of vertebrae, in the body and/or the tail (Parra-Olea and Wake, 2001; Ward and Brainerd, 2007; Bergmann and Irschick, 2012; Ward and Mehta, 2014; Ward et al., 2015). For example, increases in the number of vertebrae appear to lead to greater flexibility (Jayne, 1982), even when angles between adjacent vertebrae remain constant (Brainerd and Patek, 1998). In whales, individual vertebrae in regions that are expected be more flexible tend to have higher aspect ratios (Fish, 1998; Buchholtz, 2001; Buchholtz and Schur, 2004).

* Corresponding author.
E-mail address: gen.morinaga@okstate.edu (G. Morinaga).
[1] Current address: Department of Integrative Biology, Oklahoma State University, 501 Life Sciences West, Stillwater, OK 74078, USA.

https://doi.org/10.1016/j.zool.2019.04.003
Received 2 October 2018; Received in revised form 4 April 2019; Accepted 5 April 2019
Available online 05 April 2019
0944-2006/

Finally, elongation of different regions of the body, can lead to differences in how these regions are used in different contexts, as fish that have elongated different parts of their body adopt different kinematic strategies during locomotion on land and in water (Ward et al., 2015). Whether elongation evolved through the addition and/or elongation of vertebrae in different body regions differs by lineage, and so we would expect functional differences between lineages of snake-like species as well (Parra-Olea and Wake, 2001; Ward and Brainerd, 2007; Bergmann and Irschick, 2012).

Lineage-specific functional differences are expected between limbed lizards, limbless lizards, and snakes because their ancestral and derived vertebral morphology differs. Whereas limbless lizards have 44 to 120 vertebrae, snakes have at least 136, and sometimes over 300 vertebrae (Hoffstetter and Gasc, 1969; Lindell, 1994; Bergmann and Irschick, 2012). In addition, although both limbless lizards and snakes have modified trunk muscles when compared to limbed lizards, the extent of modification both in number and complexity are much greater in snakes than limbless lizards (Auffenberg, 1962; Hammond and Ridge, 1978; Gasc, 1981; Jayne, 1982).

Morphological differences such as vertebral number and shape contribute to how undulatory waves are propagated during locomotion (Gans, 1962, 1974, 1975, 1986), but how animals move is also partially dependent on the ecological context and how the animal interacts with its environment (Irschick and Jayne, 1998, 1999; Kohlsdorf and Wagner, 2006; Astley and Jayne, 2007; Ward et al., 2015). For example, snakes are able to employ various modes of locomotion—lateral undulation, sidewinding, rectilinear, slide-pushing, and concertina (Gans, 1962, 1974, 1984). These modes of locomotion tend to be habitat-specific, but can also be combined with one another on a single substrate (Gray, 1946; Bennet et al., 1974; Jayne, 1986; Jayne and Davis, 1991). In contrast, limbless lizards have a limited repertoire of locomotor modes and cannot use multiple locomotor modes at the same time (Gans and Gasc, 1990; Gasc and Gans, 1990; Gans et al., 1992).

The different locomotor modes used by snakes have been studied in the laboratory using parallel-sided channels and evenly-spaced arrays of pegs to mimic tunnels and structurally-complex habitats, respectively (Gray, 1946; Bogert, 1947; Lissmann, 1950; Bennet et al., 1974; Jayne, 1986; Jayne and Davis, 1991). In parallel-sided channels, snakes tend to use concertina locomotion by alternately forming and extending a series of “S” bends at the posterior and anterior ends of the body (Gans, 1962, 1974). The amplitude of these “S” bends increases in wider channels (Jayne, 1986; Jayne and Davis, 1991). Snakes use lateral undulation to push past pegs and some species are capable of combining lateral undulation with sidewinding to traverse through widely spaced peg arrays (Bennet et al., 1974; Jayne, 1986; Kelley et al., 1997). These studies show that snakes adeptly modulate locomotor mode and axial kinematics to move through both structurally-complex habitats and narrow tunnels.

Similar experiments on limbless anguimorph lizards (*Ophisaurus apodus, Anguis fragilis,* and *Anniella pulchra*) found that they only engage in simple undulatory locomotion in peg arrays, while in channels they rely exclusively on a variant of concertina called continuous bend concertina (Gans and Gasc, 1990; Gasc and Gans, 1990; Gans et al., 1992). During continuous bend concertina, the whole body alternates between forming and extending a series of few, long “S” bends (Gans and Gasc, 1990; Gasc and Gans, 1990). While these qualitative studies have been important in understanding how limbless squamates move, none have quantitatively compared locomotion of limbed lizards to limbless lizards and snakes. Thus, it remains unknown how limbless lizards and snakes differ in their locomotor kinematics and whether these differences have implications for the evolution of limbless locomotion.

Here, we compare the locomotor kinematics of a limbed lizard, which represent the ancestral body shape of squamates, a limbless lizard, and a snake. We do so, not to draw any evolutionary or ecological comparisons between the species, but to compare their kinematics and relate those to vertebral and body shape differences. We do this using both high-speed X-ray and light video to quantify and compare gross axial kinematics and vertebral kinematics as these animals traverse different channel widths and arrays of different peg densities. We study axial kinematics using three fundamental wave properties: amplitude, wavelength, and frequency. Amplitude is the lateral displacement of a marker on the body from the path of the animal, wavelength is the distance between adjacent undulatory peaks, and frequency is the inverse of time between undulatory peaks.

To elucidate what locomotor kinematic differences exist between limbed lizards, limbless lizards, and snakes, we test three hypotheses. First, we test the hypothesis that vertebral dimensions differ between the three focal species. We predict that because snakes have more vertebrae than lizards (Bergmann and Irschick, 2012), they will have vertebrae with smaller aspect ratios than either of the lizard species (Gomez et al., 2008). Second, we test the hypothesis that limbed lizards, limbless lizards, and snakes differ in their vertebral and axial kinematics. We predict that the two lizard species will have similar intervertebral joint angles at the apex of a bend, and that these joint angles will be greater than in the snake because of the similarity in vertebral aspect ratios (Buchholtz, 2001; Buchholtz and Schur, 2004). We also predict that the limbless lizard and snake will exhibit similar axial kinematics in the peg array treatments because both rely on axial locomotion (Gray, 1946; Gans and Gasc, 1990). However, we expect their axial kinematics to differ in channel treatments owing to differences in how concertina is performed by limbless lizards and snakes (Gray, 1946; Gans and Gasc, 1990). Third, we test the hypothesis that amplitude, wavelength, and frequency covary with one another during undulatory locomotion. Although a number of studies have quantified undulatory kinematics (Gray, 1946; Jayne, 1985; Gillis, 1998; Maladen et al., 2009; Pace and Gibb, 2011), it is unknown how amplitude, wavelength and frequency are related. Intuitively, increases in the spatial components of the undulatory wave (i.e., amplitude and wavelength) should have an inverse relationship with frequency because a marker must travel a greater distance during each undulation. Thus, we predict that for all species, increasing either amplitude or wavelength will lead to a decrease in frequency.

2. Methods

2.1. Animals studied and husbandry

We used three Fire Skinks (*Riopa fernandi*), four European Glass Lizards (*Ophisaurus apodus*), and four Northern Water Snakes (*Nerodia sipedon*), all obtained from a commercial dealer (see Table 1 for body size measurements). We housed the animals singly or in pairs in glass

Table 1
Sample size (n), average measurements and standard errors of snout–vent length (SVL), body width (BW), TL (total length), elongation ratio (ER), median pre-cloacal (PCV) and caudal vertebral (CV) counts, and estimated marginal mean aspect ratios for the mid-body vertebrae (VAR) for the three focal species of this study. All length measurements are in mm.

Species	n	SVL	BW	TL	ER	PCV	CV	VAR
R. fernandi	3	136.60 ± 3.24	23.81 ± 1.09	262.55 ± 15.87	11.02 ± 0.27	32	28	1.07 ± 0.02
O. apodus	4	325.20 ± 9.49	28.09 ± 1.51	808.53 ± 3.99	28.99 ± 1.28	59	88	1.04 ± 0.01
N. sipedon	4	469.84 ± 32.69	21.64 ± 0.32	663.62 ± 29.47	30.71 ± 1.57	135	46	0.84 ± 0.02

terraria (51 × 10 × 32 cm, single animal; 91 × 45 × 42 cm, pair of animals, L x W x H). We provided wood shavings for *R. fernandi*, and a mixture of dried leaf litter and vermiculite for substrate for *O. apodus* and *N. sipedon*. We fed *R. fernandi* three to five crickets and *O. apodus* commercially available wet cat food supplemented with one to two crickets every two days. We fed *N. sipedon* two to three feeder fish once a week. We provided all animals with water ad libitum by misting their cages and providing water dishes (0.75 L for *R. fernandi* and *O. apodus*, 3 L for *N. sipedon*). We kept the animals in a room with an ambient temperature of 24°–27 °C and under-tank heaters to provide a thermal gradient. We set the room to a 12:12 light:dark cycle, and provided each terrarium with a UV-B light bulb. The Clark University Institutional Animal Care and Use Committee approved all husbandry and experimental procedures.

2.2. Preparing animals for X-ray trials

We performed all trials at least 48 hours after feeding. Prior to starting trials, we painted landmarks on the dorsal surface of the animal at the occiput, mid-body, and cloaca using a non-toxic white paint pen. Once the paint dried, we used super glue (Pacer Technology, Rancho Cucamonga, CA, USA) to adhere 1 × 1 mm radio-opaque markers on top of the painted markers. When the glue dried, we placed each animal individually in a cloth bag and placed them in an incubator set at 33 °C for at least 15 minutes before each trial.

2.3. Recording high-speed video of animals moving through channels and peg arrays

We subjected each animal to three trials in each treatment, which included an open control treatment and treatments of different channel widths and peg densities. We conducted all trials in a plastic, radio-translucent racetrack (122 × 30 × 22 cm, L × W × H) lined with fiberglass mesh to provide traction. The open control was an unobstructed, 30 cm wide racetrack. The channel treatments partitioned the racetrack lengthwise to 4, 6, and 15 cm wide. The peg treatments varied in density of pegs: 839 pegs/m^2 (spaced 20 mm apart from edge to edge of pegs), 419 pegs/m^2 (spaced 50 mm apart), 97 pegs/m^2 (spaced 80 mm apart), and 75 pegs/m^2 (spaced 110 mm apart). For a schematic of these treatments see Supplementary Fig. 1. Each peg was 16.1 mm high and 9.6 mm in diameter. For all trials, we encouraged animals to move along the length of the track by gently tapping their tail or hind limb with a long wooden dowel. We considered the trial completed when the animal traversed the length of the racetrack and crossed the field of view of the high-speed X-ray and light cameras.

We recorded each trial using a high-speed X-ray video system (Series 9400, OEC Medical Systems Inc., Salt Lake City, UT, USA) with a 30 cm image intensifier (Dunlee Image Intensifier Assembly, Arlington, TX, USA). We imaged the animals at X-ray settings of 66-68 kVp and 6.7 mA. We recorded videos at 250 frames/s using an A-X-Streme Vision XS-5 high-speed camera (IDT Vision, Tallahassee, FL, USA) equipped with a Nikon AF Micro-Nikkor 60 mm f/2.8 D macro lens (Nikon Corporation, Tokyo, Japan). We simultaneously imaged the animals from dorsal view at 240 frames/s using an ordinary high-speed video camera (EX-ZR100, Casio, Tokyo, Japan). We used the high-speed X-ray video to visualize vertebral kinematics at the mid-body marker, and the ordinary high-speed video to visualize axial kinematics for each marker. We placed a US 25 cent coin (24.26 mm diameter) in the field of view of both cameras to serve as a scale object. We additionally took X-ray still images of the specimens using a veterinary X-ray imaging system (ROTANODE E7242X, Toshiba Electron Tubes & Devices Corporation, Otawara City, Japan) at 66–68 kVp and 6.7 mA. We used SimonDR (version 4.0.14963, DMMD, Arlington, VA, USA). These images were higher resolution than that of the videos and allowed us to accurately count the number of vertebrae in the vertebral column of each specimen.

2.4. Video processing and quantification

Images captured using X-ray video systems are distorted (Wang and Blackburn, 2000) and must be corrected prior to analysis. We corrected X-ray videos using XrayProject version 2.2.7 (Brainerd et al., 2010) for MatLab version 2015a (MathWorks, Natick, MA, USA). To correct the distorted image, we recorded an x-ray video of a calibration grid prior to the start of every session. This calibration grid was a steel sheet with 3.18 mm perforations spaced 4.76 mm apart in a staggered arrangement (Brainerd et al., 2010). XrayProject uses a distortion correction algorithm to calculate a transformation matrix, which is used to undistort each video.

To quantify vertebral kinematics, we measured intervertebral joint angles at the mid-body marker for each X-ray video using ImageJ (Schneider et al., 2012). To do this, we first identified the frame at which the greatest bend occurred by eye. Then we identified the centers of three consecutive vertebrae at the apex of the bend by eye, and measured the angle between those three vertebrae using the 'Angle Tool'. To ensure that we captured the greatest vertebral angle, we measured the angle between the same three vertebrae in ten preceding frames and in nine subsequent frames, for a total of 20 consecutive frames. These angles spanned two intervertebral joints, so we divided them by two.

We quantified amplitude, wavelength, and frequency based on the motion of each body marker using ordinary high-speed video. Amplitude is the deviation of a marker from a straight-line path, wavelength is the Euclidean distance between undulatory peaks, and frequency is the inverse of the time difference between undulatory peaks. To quantify these axial kinematics, we first tracked the motion of the each marker using DLTdv5 (Hedrick, 2008) for MatLab. Because DLTdv5 outputs pixel coordinates indexed by frame number, we converted these data to millimeter coordinates using a conversion factor obtained from measuring the diameter of a US 25 cent coin using the 'Set Scale' function in ImageJ because these were dorsal images. We then used code that we wrote for R version 3.3.1 (R Core Team, 2016) to calculate amplitude, wavelength, and frequency for each marker using the coordinate data. This code modeled the path of the animal as a straight line using a simple linear regression of the *x-y* coordinates of the occiput (anterior-most) marker. The code then calculated the residual deviation of each marker, including the occiput, from the regression (Fig. 1). These residuals represented the undulatory motion of each marker along the modeled linear path. The code then identified local extrema (peaks and valleys) in a three-step process. First, the code identified local extrema and checked for more extreme values within intervals of 30 frames before and after them. If a more extreme value occurred within this interval, the original extremum was considered a false peak or valley and not counted. Next, the extrema identified from the first step were thresholded to further remove false peaks and valleys such that the absolute-value difference between two adjacent extrema (a peak and a valley) was greater than one standard deviation of the full sequence of marker residuals. The last step checked to ensure that the sequence of extrema was alternating (i.e., maximum-minimum-maximum or minimum-maximum-minimum). The code used the identified extrema to calculate amplitude, wavelength, and frequency. Amplitude was the average of the absolute values of residuals of all extrema for a marker. Wavelength was the average Euclidean distance that a marker moved between consecutive maxima and consecutive minima. Frequency was the average inverse of the duration of time between consecutive maxima and consecutive minima (Fig. 1). Our dataset (Supplementary Table S2) and the code used to detect local minima and maxima (Supplementary Code S3) are available as supplementary online materials.

We obtained all morphometric measurements from either the X-ray videos, the light videos, or an X-ray still image of the specimens using ImageJ. After using the 'set scale' function, we used the 'straight line' tool and measured the length and width of the three vertebrae that we

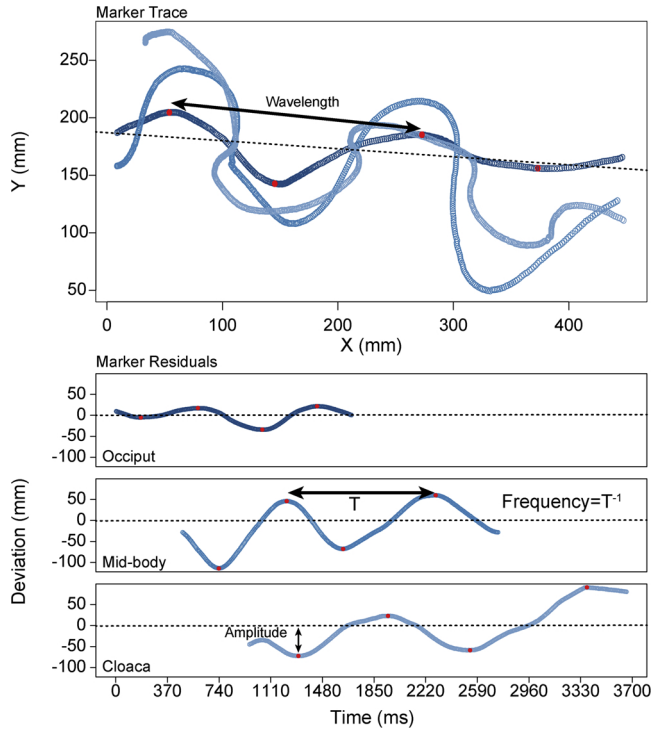

Fig. 1. A sample plot of marker traces in *x*-*y* space and marker residuals against time for a trial of *Nerodia sipedon* moving through the control treatment, showing how axial kinematic variables were quantified. The blue lines indicate marker position, with darker colors being more anterior and lighter colors being more posterior. Red circles indicate the local extrema identified by our R code. Dotted black lines show the path taken by the animal modeled using ordinary least squares regression on the *x*-*y* points of the occiput marker.

had measured intervertebral joint angles for in the X-ray videos. We calculated vertebral aspect ratio by dividing vertebral length by width. We used the 'free hand' tool to measure snout–vent length and total length, and used the 'straight line' tool to measure body width. We then calculated elongation ratio by dividing total length by body width (Ward and Azizi, 2004). Finally, we counted the number of pre-cloacal vertebrae and caudal vertebrae from an X-ray still image of each specimen. These measurements are summarized in Table 1.

2.5. Statistical Analysis

We performed all statistical analyses using R version 3.3.1 (R Core Team, 2016). We used linear mixed models as implemented in the lme4 package (Bates et al., 2015) for R. We used linear mixed models because we included multiple trials per individual, and linear mixed models allowed us to account for this non-independence by including individual (n = 11) as a random effect. We fitted all models using restricted maximum likelihood. We first modeled the effect of species on vertebral aspect ratios. We did this by including vertebral aspect ratio as the response variable, species as fixed effects, and individual as a random effect. Next, we modeled the effect of species and treatment levels on intervertebral joint angles during locomotion. Here, we used intervertebral joint angle at the mid-body marker as the response variable, species, treatment level, and their interaction as fixed effects, and individual as a random effect. Then, we modeled the effect of species and treatment levels on amplitude, wavelength, and frequency. We used each of the ln-transformed kinematic traits as response variables, species, marker position, treatment level, and all two-way interactions except for the interaction between marker position and treatment level as fixed effects, and individual as a random effect. We ran separate analyses for channel treatments (four levels) and peg-array treatments (five levels). Finally, we tested whether axial kinematic traits interacted with one another and whether these interactive effects differed between species. For this, we used ln-transformed frequency as the response variable, ln-transformed amplitude and wavelength, species, and all possible two-way interactions except the interaction between amplitude and wavelength as fixed effects, and individual as a random effect. To help visualize these relationships, we then used this model to predict the effect of ln-transformed wavelength on ln-transformed frequency while fixing ln-transformed amplitude at three levels: the species mean and species mean ± one standard deviation (*R. fernandi:* 2.62 ± 0.55; *O. apodus:* 4.37 ± 0.56; *N. sipedon:* 4.05 ± 0.51). For this last analysis, we only considered measurements from the control treatment. We did not include body size in our analyses because interspecific differences in body size were much greater than intraspecific differences, and the species identity perfectly masked these differences (Table 1). Hence, we consider possible effects of body size in the discussion.

We assessed effect sizes for the fixed and random effects by calculating marginal and conditional R^2 using the R package MuMIn (Bartoń, 2018). Marginal R^2 (R^2_M) is the variance explained by only the fixed effects, while conditional R^2 (R^2_C) is the variance explained by both fixed and random effects (Nakagawa and Schielzeth, 2013; Bartoń, 2018). We then estimated post-hoc marginal means as implemented in the emmeans package (Lenth, 2019). These marginal means were estimated from the parameters of the fitted models, which included both fixed and random effects (Searle et al., 1980).

We tested our hypotheses by comparing marginal means between a priori defined combinations of species, treatment, and marker position and tested for differences. Specifically, we tested whether vertebral aspect ratios differed between species. We then tested whether species exhibited different intervertebral joint angles from one another within each treatment level and whether each species exhibited different intervertebral joint angles across different treatment levels. For each of the axial kinematic traits, we tested whether species differed from one another within a treatment level, whether axial kinematic traits changed for each species in different treatment levels, and whether axial kinematic traits differed at each marker for each species within in a treatment level. For species and treatment comparisons, we calculated the average for each axial kinematic trait across the three markers for each species in each treatment prior to making the comparison. This resulted in over 500 comparisons, so we only present the range of significant *p*-values, the total number of significant *p*-values, and the total number of comparisons for each kinematic variable (Tables S4–S6). In the main text, we present the highest significant *p*-value (p_{HS}), which represents the weakest evidence in support of each statement of a difference. Because the pattern of marker differences did not change in any of the three species across differing levels of either peg or channel treatments, we present marker differences of the least restricted treatments (i.e., 15 cm channel, 75 pegs/m^2) in the main text (Figs. 4 and 5), and marker comparisons for the other treatments in the supplementary online material (Figs. S7 and S8). Finally, to assess the significance of the interactive effects of axial kinematic traits on one another across species, we used the R package lmerTest (Kuznetsova et al., 2017) because lme4 does not natively calculate *p*-values (Bates et al., 2015).

3. Results

3.1. Elongation ratio, vertebral number vertebral aspect ratio, and intervertebral joint angle

We found *Nerodia sipedon* and *Ophisaurus apodus* exhibited similar elongation ratios, while *Riopa fernandi* had the lowest (Table 1). There were significant differences in vertebral number and aspect ratio between the three species (Table 1). *Riopa fernandi* had the fewest precaudal and caudal vertebrae, while *O. apodus* the most caudal

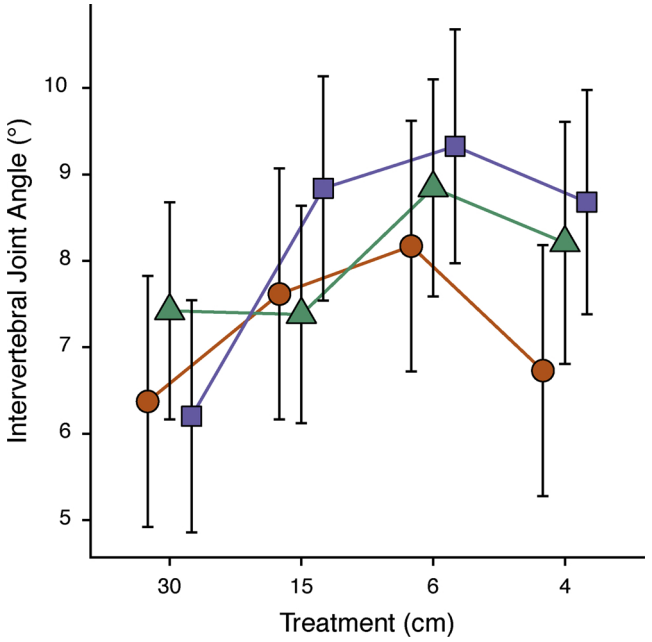

Fig. 2. Comparison of marginal means of intervertebral joint angles estimated from the linear mixed models for channel treatments. The different colors, shapes and lines represent different species (orange circles and lines: *Riopa fernandi*, green triangles and lines: *Ophisaurus apodus*, purple squares and lines: *Nerodia sipedon*). The 30 cm channel is the control treatment. Error bars are standard errors.

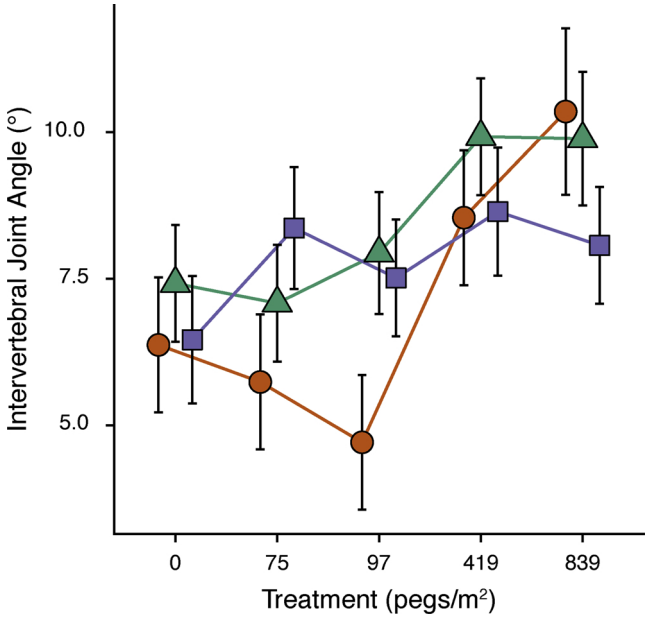

Fig. 3. Comparison of marginal means of intervertebral joint angles estimated from the linear mixed models for peg-array treatments. The different color shapes and lines represent different species (orange circles and lines: *Riopa fernandi*, green triangles and lines: *Ophisaurus apodus*, purple squares and lines: *Nerodia sipedon*). The 0 pegs/m^2 treatment is the control treatment. Error bars are standard errors.

vertebrae, and *N. sipedon* had the most pre-caudal vertebrae (Table 1). Vertebral aspect ratios for the two lizard species were significantly greater than those of the snake at the mid-body ($p_{HS} < 0.0001$, Table 1, Table S3). Notably, the vertebrae of the two lizard species had aspect ratios slightly, but significantly, greater than one, while *N. sipedon* had significantly shorter and wider vertebrae (Table 1). For this model, fixed effects explained 82% of variance ($R^2_M = 0.816$) and random effects explained none of the variance in the data ($R^2_C = 0.816$).

Across different channel widths, the three species used similar intervertebral joint angles at the mid-body (Fig. 2, Table S3). In the peg array treatments, both elongate species showed a slight, non-significant increase in joint angle as peg densities increased (Fig. 3, Table S3). *Riopa fernandi* used significantly greater intervertebral joint angles in the 419 and 839 pegs/m^2 treatments than in the two lowest density peg treatments ($p_{HS} = 0.0363$, Fig. 3, Table S3). The three species did not significantly differ from one another in most treatments with the exception of the 97 pegs/m^2 treatment, where *R. fernandi* exhibited significantly lower intervertebral joint angles than either of the elongate species ($p_{HS} = 0.0408$, Fig. 3, Table S3). These models explained less variance than other models presented. The fixed effects of species, treatment, and markers explained only about 6% and 16% of variance in intervertebral joint angle for channel and peg treatments, respectively, and the random effect of individual explained an additional 13% and 2%, respectively (Table 2).

3.2. Axial kinematics in parallel-sided channels

Our findings showed that undulatory amplitude decreased as channels narrowed in all three species and that both elongate species consistently used larger amplitudes than *R. fernandi* (Fig. 4 A). In the wider channels, *O. apodus* used greater amplitudes than *N. sipedon*, but this switched in the narrower channels and *O. apodus* used significantly smaller amplitudes ($p_{HS} = 0.0172$, Fig. 4A, Table S4). For *R. fernandi*, amplitudes did not significantly differ between the two wider channels or between the two narrower channels, although differences between wide and narrow were significant ($p_{HS} = 0.0077$, Fig. 4A, Table S4). All three species showed a tendency to significantly increase amplitude posteriorly ($p_{HS} = 0.0204$, Fig. 4B, Table S4, Fig. S6). The fixed effects in this model (species, treatment, and marker position) explained 76% of variance in the data, while the random effect of individual explained an additional 2% (Table 2).

Wavelengths tended to decrease as channels narrowed for all three species (Fig. 4C). In most treatments, *O. apodus* exhibited the shortest wavelengths ($p_{HS} = 0.0387$, Fig. 4C, Table S4), while *R. fernandi* and *N. sipedon* did not differ significantly from one another in any channel width. When we considered wavelengths at each marker position, each species exhibited a distinct pattern. *Riopa fernandi* exhibited no differences in wavelength across markers, and *O. apodus* used significantly longer wavelengths at the mid-body marker than either occiput or cloaca markers ($p_{HS} = 0.0047$, Fig. 4D, Table S4, Fig. S6). *Nerodia sipedon* showed significantly longer wavelengths posteriorly, as the occiput had the shortest wavelength ($p_{HS} = 0.0047$, Fig. 4D, Table S4, Fig. S6). The fixed effects for this model explained 58% of variance, while the random effect of individual explained an additional 1% (Table 2).

Across all channel widths, *R. fernandi* exhibited greater frequencies than either elongate species ($p_{HS} = 0.0149$, Fig. 4E, Table S4). The two lizard species exhibited significant increases between the 15 and 6 cm channels, while *N. sipedon* exhibited a significant decrease between the 15 and 6 cm channels ($p_{HS} = 0.0471$, Fig. 4E, Table S4). Marker trends in frequency differed by body shape. While *R. fernandi* exhibited no frequency differences between marker positions, both elongate species exhibited significantly higher frequencies at the occiput ($p_{HS} = 0.0324$, Fig. 4F, Table S4, Fig. S6). Fixed effects in this model explained 57% of the variance and the random effect of individual explained another 7% (Table 2).

3.3. Axial kinematics in arrays of pegs

Across most peg densities, the two elongate species exhibited greater amplitudes than *R. fernandi* (Fig. 5 A). The only exception to this was in the 839 pegs/m^2 treatment, where *O. apodus* exhibited

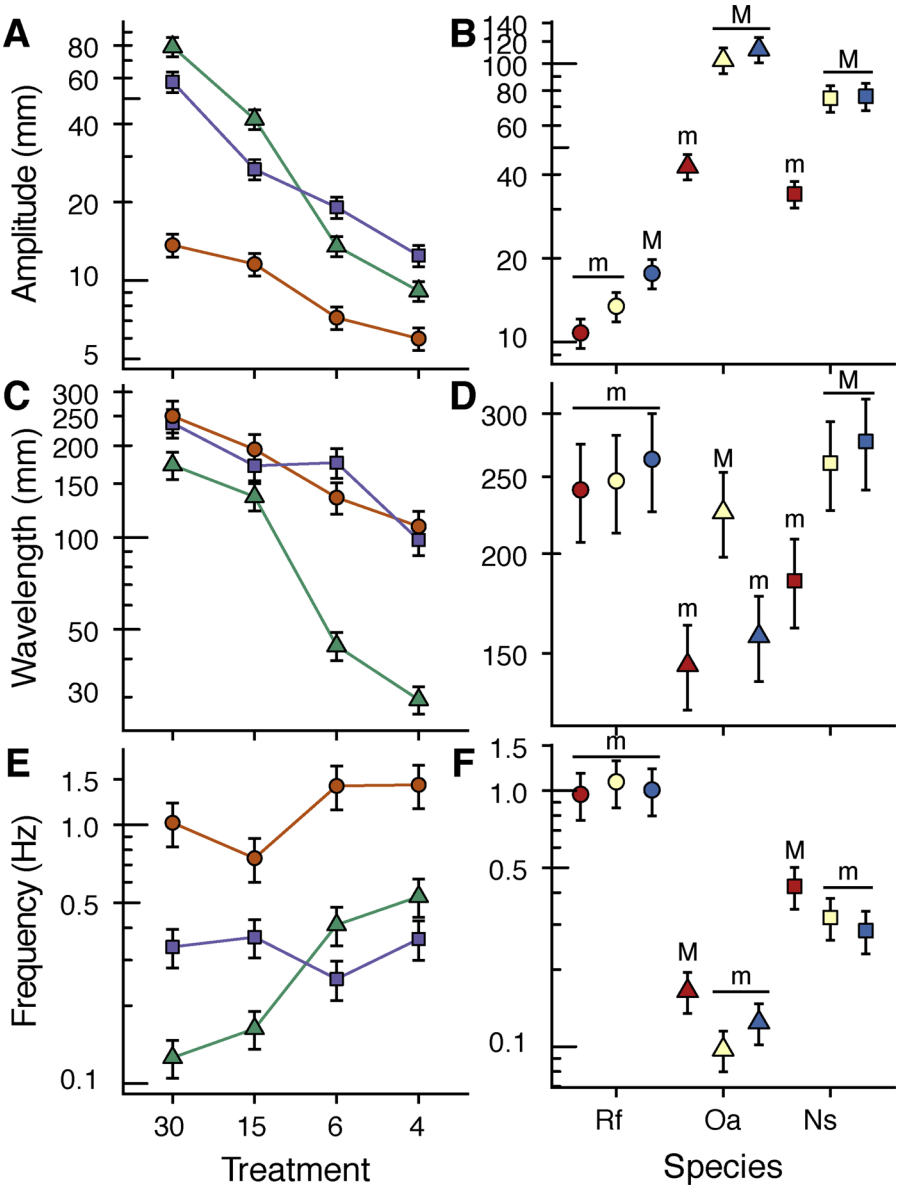

Fig. 4. Comparisons of back-transformed marginal means estimated from linear mixed models of ln-transformed axial kinematic traits in channel treatments. A, C and E: Marginal means for each species averaged across markers for each treatment (orange circles and lines: *Riopa fernandi*, green triangles and lines: *Ophisaurus apodus*, purple squares and lines: *Nerodia sipedon*). The 30 cm channel is the control treatment. B, D and F: Marginal means for each marker (red: occiput, yellow: mid-body, blue: cloaca) on each species (circles: *R. fernandi*, triangles: *O. apodus*, squares: *N. sipedon*) in the 15 cm channel treatment. Letters above shapes indicate groupings of significantly different markers within each species. Horizontal bars connect markers that are not significantly different. All error bars are standard errors. For all plots, the *y*-axis is in log scale.

amplitudes as low as *R. fernandi* (Fig. 5A, Table S5). Across treatments, only *O. apodus* exhibited a steady decrease in amplitude (p_{HS} = 0.0437, Fig. 5A, Table S5). Of the other two species, in *R. fernandi* amplitudes did not change across treatments except for a significant decrease in the 839 pegs/m^2 (p_{HS} = 0.0437, Fig. 5A, Table S5). In *N. sipedon* amplitudes did not differ across peg densities. Amplitudes increased for more posterior markers for all three species, with the occiput for each species exhibiting the lowest amplitudes (p_{HS} = 0.0437, Fig. 5B, Table S5, Fig. S7). Fixed effects explained 57% of variance in amplitude, while the random effect of individual explained an additional 3% (Table 2).

Wavelengths did not differ across peg densities for any of the three species, except in the 839 pegs/m^2 treatment (Fig. 5C). In that treatment, *N. sipedon* exhibited significantly longer wavelengths than either lizard species, and *O. apodus* exhibited the shortest wavelengths (p_{HS} = 0.0402, Fig. 5C, Table S5). *Riopa fernandi* and *N. sipedon* exhibited similar wavelengths between markers, while *O. apodus* had significantly shorter wavelengths for the occiput than the more posterior markers (p_{HS} = 0.0052, Fig. 5D, Table S5, Fig. S7). The fixed effects in this model explained 43% of wavelength variance, while the random effect of individual explained 2% more (Table 2).

Riopa fernandi exhibited higher frequencies across all peg densities than either elongate species (Fig. 5E). The three species showed little variation across peg densities, with the exception of *O. apodus* in the control treatment, where frequencies were significantly lower than in all other peg densities (p_{HS} = 0.0162, Fig. 5E, Table S5). *Riopa fernandi* and *N. sipedon* showed no differences in frequency between marker positions, but *O. apodus* exhibited higher frequencies at the occiput than at the mid-body or cloaca markers (p_{HS} = 0.0037, Fig. 5F, Table S5, Fig. S7). Fixed effects explained 32% of variance in frequency data, while the random effect of individual explained an additional 8% (Table 2).

3.4. Relationships between axial kinematic parameters

The fixed effects of species, amplitude, and wavelength accounted for about 65% of the variance in wave frequency, while random effects accounted for another 19% (R^2_M = 0.652, R^2_C = 0.840). *Riopa fernandi* used the highest undulatory frequency overall, followed by *N. sipedon* and *O. apodus* (Table 3; Fig. 6). Amplitude was not significantly related to frequency for any of the three species (Table 3; Fig. 6). In contrast, wavelength was significantly negatively related to frequency for all three species, but these effects did not differ between species (Table 3; Fig. 6).

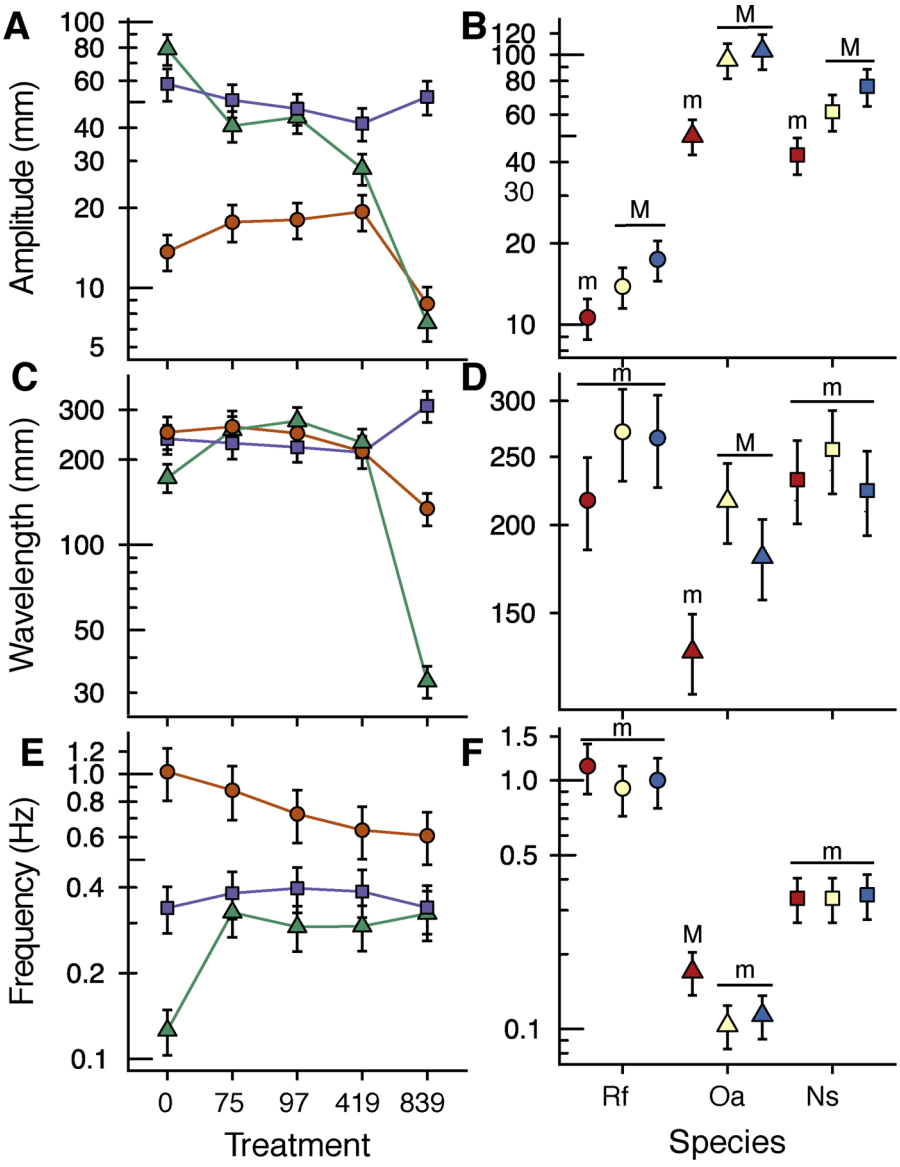

Fig. 5. Comparisons of back-transformed marginal means estimated from linear mixed models of ln-transformed axial kinematic traits in peg-array treatments. A, C, and E: Marginal means for each species averaged across markers for each treatment (orange circles and lines: *Riopa fernandi*, green triangles and lines: *Ophisaurus apodus*, purple squares and lines: *Nerodia sipedon*). The 0 pegs/m^2 treatment is the control treatment. B, D and F: Marginal means for each marker (red: occiput, yellow: mid-body, blue: cloaca) on each species (circles: *R. fernandi*, triangles: *O. apodus*, squares: *N. sipedon*) in the 75 pegs/m^2 treatment. Letters above shapes indicate groupings of significantly different markers within each species. Horizontal bars connect markers that are not significantly different. All error bars are standard errors. For all plots, the *y*-axis is in log scale.

Table 2
Marginal and conditional coefficients of determination (R^2_M and R^2_C) of the linear mixed models for vertebral and axial kinematic measurements. R^2_M is variance explained by fixed effects while R^2_C is variance explained by random effects.

	Channel		Peg	
Response variable	R^2_M	R^2_C	R^2_M	R^2_C
Intervertebral joint angle	0.061	0.196	0.158	0.185
Amplitude	0.757	0.760	0.572	0.603
Wavelength	0.579	0.590	0.428	0.453
Frequency	0.572	0.641	0.320	0.405

Table 3
Intercept and partial-slope estimates for the linear mixed model testing for relationships of amplitude and wavelength with frequency for each species. The estimates are the actual intercepts and partial slopes for each species, but the t-statistics and P-values for *O. apodus* and *N. sipedon* (shaded in gray) are tests of differences from *R. fernandi*, which the analysis used as a reference. Amplitude, wavelength, and frequency were all ln-transformed prior to analysis. Significant *p*-values are in bold.

Parameter	Species	Estimate ± SE	t	*p*
Intercept	*R. fernandi*	5.77 ± 1.37	4.91	< **0.0001**
	O. apodus	1.94 ± 0.76	−1.58	**0.0128**
	N. sipedon	2.38 ± 1.15	−2.21	**0.0409**
Amplitude	*R. fernandi*	−0.04 ± 0.22	−0.16	0.8584
	O. apodus	−1.06 ± 0.30	−1.14	0.1628
	N. sipedon	0.15 ± 0.27	0.73	0.5198
Wavelength	*R. fernandi*	−1.02 ± 0.29	−4.06	**0.0009**
	O. apodus	−0.42 ± 0.31	0.80	0.0565
	N. sipedon	−0.75 ± 0.36	0.90	0.4540

4. Discussion

Although many studies have quantified the locomotor kinematics of limbless animals (Jayne, 1982, 1986; Renous and Gasc, 1989; Gans and Gasc, 1990; Gasc and Gans, 1990; Jayne and Davis, 1991; Gans et al., 1992; Summers and O'Reilly, 1997; Moon and Gans, 1998; Moon, 1999; Astley and Jayne, 2007), we still lack an understanding of how locomotor kinematics differ between elongate forms with different underlying morphologies from limbed, non-elongate forms (but see Ward et al., 2015). Here, we investigated the undulatory kinematics of two independently evolved elongate limbless squamates that differed in vertebral number and morphology and compared them to that of a limbed species that represented the ancestral body shape. Of the three species we studied, *Riopa fernandi* had the lowest elongation ratio,

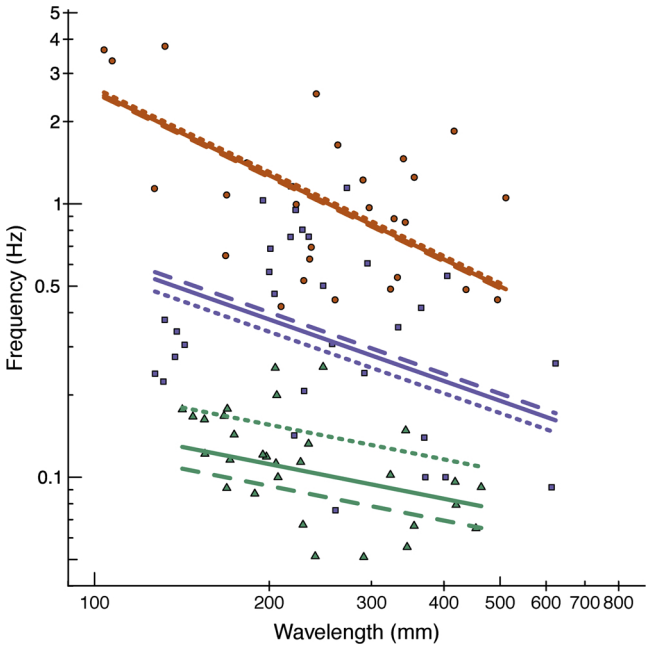

Fig. 6. The effect of wavelength on frequency for *Riopa fernandi* (orange circle and lines), *Ophisaurus apodus* (green lines and triangles), and *Nerodia sipedon* (purple line and squares) at three fixed levels of amplitude: the species mean (solid lines), species mean + 1 SD (dotted lines), species means-1 SD (dashed lines). All axial kinematic traits were ln-transformed for model fitting and were back transformed. Both *x*- and *y*- axes are in log scale.

while the two elongate species exhibited similar elongation ratios despite the snake having a relatively longer SVL than the limbless lizard (Table 1). We found that the snake had substantially more trunk vertebrae that were relatively shorter than either lizard species (Table 1). We found no differences in intervertebral joint angles during locomotion through channels (Fig. 2), and gradual increases in angles as peg densities increased in the two lizard species (Fig. 3). Our findings also showed all three species modulated their axial kinematics in channel and peg treatments and these patterns differed among species and treatment levels (Figs. 4 and 5). Lastly, we found that undulatory frequency changed with wavelength, but not amplitude in all three species (Fig. 6). These results indicate a decoupling of axial kinematic variables in all three species, but the underlying mechanisms are likely different between elongate and non-elongate forms. The combination of decoupling and greater localized flexibility resulting from musculoskeletal differences likely facilitated diversification of locomotor strategies in snakes but not limbless lizards.

4.1. Differences in vertebral column morphology and intervertebral joint angles

Vertebral number or aspect ratios affect the flexibility of the vertebral column in snakes (Jayne, 1982), fishes (Brainerd and Patek, 1998), and are suspected to do so in cetaceans (Buchholtz, 2001; Buchholtz and Schur, 2004). Previous work on vertebral torsion in gopher snakes (*Pituophis melanoleaucus*) showed that morphological features such as pre- and post-zygopophyses, zygosphenes, and zygantra limit torsional angles to a mere 2.19° per intervertebral joint, but this results in a large additive effect because a single bend can span 10 intervertebral joints (Moon, 1999). Pre- and post-zygapophyses may similarly act to limit lateral bending at each intervertebral joint (Hoffstetter and Gasc, 1969), but may have large additive effects as more joints participate in a single lateral bend. We did not measure the size of these processes, and a future study taking these structures into account could further elucidate their effects at individual intervertebral joints. While all three species that we studied exhibited similar angles at individual joints, *N. sipedon* should be most flexible overall because they have more vertebrae that are relatively shorter than either lizard species. Our axial kinematic results support this idea because *N. sipedon* exhibited the greatest amplitudes of the three species in the most constrained treatment levels (Figs. 4A and 5 A). In fact, in the peg array treatments, we found that *N. sipedon* showed no variation in amplitude. This could indicate that having many small vertebrae enabled the snake to maintain similar amplitudes and use greater bends (Table 1; see also Jayne, 1982), unlike *O. apodus,* which had to employ a different kinematic strategy in the 839 pegs/m^2 treatment.

Our study showed context-dependent differences in the intervertebral joint angles that were achieved by the two lizard species as they moved through channels that varied in width. While we found no differences in intervertebral joint angles between channel widths for any species (Fig. 2), greater peg densities gradually led to greater intervertebral joint angles in both lizard species (Fig. 3). In contrast, *N. sipedon* showed no differences in intervertebral joint angles in both channel and peg array treatments. To our knowledge, we are the first to document context-dependent intervertebral joint angles in squamates, although it has been documented that the American eel (*Anguilla rostrata*) and mudskippers (*Periophthalmus argentilineatus*) use greater intervertebral joint angles during terrestrial than aquatic locomotion (Gillis, 1998; Swanson and Gibb, 2004). Why the two lizards showed differences in intervertebral joint angles in different treatments, but the snake did not may be due to a combination of factors. First, locomotor kinematics are likely to change when the animal is presented with obstacles along its path of travel (Walter, 2003; Kohlsdorf and Biewener, 2006). For *R. fernandi*, denser peg-array treatments may have required changes in vertebral kinematics because forward progression required that each animal maneuver around individual pegs. In contrast, locomotion through channels and less dense peg-arrays might require less maneuvering because fewer changes in direction are needed, and thus less bending. Second, *O. apodus* likely used a similar strategy to *R. fernandi*, whilst also having to bend the body to make forward progression (Gans, 1962, 1974, 1975). Third, *N. sipedon* had many more, shorter vertebrae and a thinner body than either lizard species (Table 1). Increasing the number of joints that can participate in a bend can help to achieve tighter bends (Jayne, 1982), while a more gracile body will be less restricted in narrower passages.

4.2. Context dependency of limbless modes of locomotion

The elongate taxa in our study used different modes of locomotion in channels and arrays of pegs. In channel treatments, elongate species used a variant of concertina locomotion, while in the peg-arrays, *O. apodus* used simple undulations (except in the 839 pegs/m^2 treatment) and *N. sipedon* used lateral undulations (G. Morinaga, personal observation). Past studies in snakes and limbless lizards similarly documented these tendencies (Mosauer, 1932; Gray, 1946; Jayne, 1986; Gans and Gasc, 1990; Gasc and Gans, 1990; Gans et al., 1992) and their specificity lends support to the idea that each limbless locomotor mode evolved as a kinematic strategy for negotiating different types of habitat structure. However, despite adopting similar kinematic strategies, each species executed each mode somewhat differently. First, concertina locomotion in both species included the characteristic series of “s” curves, but localization of these bends differed. In *O. apodus*, the “s” bends continued along the entire length of the animal and the whole body alternated between lengthening and shortening. In *N. sipedon*, the bends were localized to either anterior or posterior portions of the body, and alternately lengthened or shortened. In peg treatments, although both simple and lateral undulations had long wavelengths and low frequencies (Fig. 5C, E), how each species contacted the pegs differed. In *O. apodus*, peg contact appeared tangential and the body did not deform around the peg. In contrast, *N. sipedon* deformed their body around each peg. The differences we observed in execution of these

kinematic strategies likely arises because of musculoskeletal differences between *O. apodus* and *N. sipedon* (Auffenberg, 1962; Hoffstetter and Gasc, 1969; Gasc, 1981). However, muscle activity patterns are unknown for any limbless lizard, and further study would be necessary to test which muscles are active and the locomotor context in which they are activated.

4.3. Kinematic strategies of different body shapes

The correlated elongation of the body and loss of limbs has functional implications, as propulsion shifts from the limbs to the body and the animal must rely more heavily on body undulations (Gans, 1962, 1974, 1975). This shift in kinematic strategy is well documented in fishes and squamates. For less elongate, carangiform (e.g., chub mackerel, *Scomber japonicus*) and thunniform (e.g., kawakawa tuna, *Euthynnus affinis*) swimmers, undulations of the body are minimal and thrust is generated by oscillations of the caudal fin (Sfakiotakis et al., 1999; Donley and Dickson, 2000). On the other hand, elongate, anguilliform swimmers such as the American eel (*Anguilla rostrata*) and European eel (*A. anguilla*) use high amplitude undulations of the body that increase posteriorly (Gillis, 1996, 1998; D'Août and Aerts, 1999). Similarly in squamates, robustly limbed, non-elongate lizards like the sand fish skink (*Scincus scincus*) and the Asian water monitor (*Varanus salvator*) use only low amplitude undulations during surface terrestrial locomotion (Ritter, 1995; Maladen et al., 2009; Sharpe et al., 2013) while limbless lizards rely on high amplitude undulations (Greer, 1987; Gans and Gasc, 1990; Gasc and Gans, 1990; Gans et al., 1992). The species we studied showed similar patterns, with *R. fernandi* exhibiting smaller amplitudes than either elongate species in almost all of the treatments that we tested (Figs. 4A and 5 A). This could be the result of having a shorter body than either of the elongate taxa (Table 1) because amplitude is constrained to be less than total body length. Another possibility is that elongate, limbless species may rely on greater amplitudes than limbed species because of the undulatory nature of most limbless modes of locomotion (Gans, 1962, 1974, 1975). Furthermore, limbs in contact with the substrate likely anchor and stabilize the body, thus constraining undulations to be closer to the path of travel (Chen, 2006). This may explain why we found no relationship between amplitude and frequency in *R. fernandi* (Fig. 6, Table 3). Our findings similarly showed no relationship between amplitude and frequency for the elongate taxa. However, the underlying cause is likely different. One possibility is that by limiting or decoupling amplitude in favor of wavelength and frequency, limbless species can increase forward, rather than lateral, displacement of the body. By decoupling amplitude from wavelength and frequency, snake-like species might also be better able to modify their wave forms and employ a greater diversity of locomotor modes.

Among elongated fishes and squamates, body shapes are typically categorized into one of two extremes—long-bodied or long-tailed (Wiens et al., 2006; Ward and Brainerd, 2007; Brandley et al., 2008; Ward and Mehta, 2014; Bergmann, 2015)—and how the body is regionalized could impact kinematic strategy. Comparisons between a long-bodied fish (*Erpetoichthys calabaricus*) and a long-tailed fish (*Gymnallabes typus*) traversing aquatic and terrestrial peg-arrays showed that *E. calabaricus* contacted pegs for longer durations during terrestrial bouts than aquatic ones (Ward et al., 2015). In contrast, *G. typus* showed similar peg contact durations in both aquatic and terrestrial bouts (Ward et al., 2015). Therefore, *E. calabaricus* uses different kinematic strategies depending on environmental context (Ward et al., 2015). The two elongate species we studied can be similarly categorized, as *O. apodus* is long-tailed and *N. sipedon* is long-bodied (Table 1). In most treatment levels, our findings differ from those of Ward et al. (2015), as axial kinematics and kinematic strategies were similar between the two elongate species (Figs. 4 and 5). However, in the 839 pegs/m^2 treatment, *O. apodus* used drastically lower amplitudes and wavelengths than *N. sipedon* (Fig. 5A, C), signifying a clear shift in kinematic strategy. In all other peg densities, all *O. apodus* specimens used simple undulatory locomotion to rapidly move through the peg arrays, but in the 839 pegs/m^2 treatment, all *O. apodus* specimens resorted to whole-body concertina locomotion (G. Morinaga, personal observation). In contrast, all *N. sipedon* specimens used lateral undulations to move through all peg-array treatments (G. Morinaga, personal observation). These observations may be due to two factors. First, while *O. apodus* and *N. sipedon* exhibited similar elongation ratios, the two species have elongated different regions of the body (Table 1). These differences likely affect locomotor kinematics as osteology and musculature differ between the body and the tail (Auffenberg, 1961, 1962; Hoffstetter and Gasc, 1969). Second, *O. apodus* had wider bodies than *N. sipedon* (Table 1). This meant that peg spacing relative to body width differed substantially in the 839 pegs/m^2 as *O. apodus* specimens had ~2 mm of clearance between their bodies and the pegs, while *N. sipedon* had ~8 mm. *Riopa fernandi* exhibited body widths intermediate to the two elongate species (Table 1) and also adopted a different kinematic strategy. It achieved this by folding one pair of limbs as the body passed each peg while the other set of limbs were used to propel it forward (G. Morinaga, personal observation).

5. Conclusions

Body elongation and limb reduction is a common evolutionary pattern found in most major vertebrate lineages (Lande, 1978; Brandley et al., 2008; Ward and Mehta, 2010). The prevailing hypothesis states that snake-like bodies evolved as an adaptation to streamline the body for locomotion through granular media or structurally-complex habitats (Gans, 1973, 1974; Greer, 1990; Ward and Azizi, 2004; Mehta et al., 2010). The shift to such a body shape places emphasis on axial flexion for mobility (Bergmann and Irschick, 2010). Context-dependent shifts in how the body is bent and its interaction with the physical environment indicate that limbless locomotor modes are different kinematic strategies to negotiate different habitat types. We are the first to visualize and compare the in vivo vertebral kinematics of a limbed lizard, limbless lizard, and a snake. Our findings showed that despite differences in vertebral aspect ratio, intervertebral joint angles did not differ in most contexts in the three species we studied. Axial kinematics differed contextually between lizards and snakes, and elongate and non-elongate species. These axial kinematic traits were decoupled from one another, and this could help explain how limbless locomotor modes manifest because different wave amplitudes, wavelengths, and frequencies can be combined in different ways. However, the muscle kinematics of limbless lizards remain unknown, and would further our understanding of why locomotion of limbless lizards and snakes differs. Furthermore, O. *apodus*, which has elongated primarily through lengthening of the tail, is but one side of the snake-like lizard body continuum (Wiens et al., 2006; Brandley et al., 2008; Bergmann, 2015). To test whether there are morphological correlates with habitat specialization, a more comprehensive sampling of different snake-like species with different tail lengths and habits is necessary.

Competing Interests

We have no competing interests to declare.

Funding

This research was supported by funds from Clark University.

Acknowledgements

We thank four anonymous reviewers, S. Patek, and members of the Bergmann lab group for reading and commenting on versions of this manuscript. We thank M. Provost and V. Zhao for assistance preparing animals and recording videos. We also thank E. G. Schaper for

assistance with animal husbandry. We additionally thank J. Augusto for assistance with taking X-ray still images of the specimens. Lastly, we thank J. Dresch for advice on quantifying axial kinematics.

Appendix A. Supplementary data

Supplementary material related to this article can be found, in the online version, at doi:https://doi.org/10.1016/j.zool.2019.04.003.

References

Astley, H.C., Jayne, B.C., 2007. Effects of perch diameter and incline on the kinematics, performance and modes of arboreal locomotion of corn snakes (*Elaphe guttata*). J. Exp. Biol. 210, 3862–3872. https://doi.org/10.1242/jeb.009050.

Auffenberg, W., 1961. Additional remarks on the evolution of trunk musculature in snakes. Am. Midl. Nat. 65, 1. https://doi.org/10.2307/2422998.

Auffenberg, W., 1962. A review of the trunk musculature in the limbless land vertebrates. Am. Zool. 2, 183–190. https://doi.org/10.1093/icb/2.2.183.

Bartoń, K., 2018. MuMIn: Multi-Model Inference.

Bates, D., Mächler, M., Bolker, B., Walker, S., 2015. Fitting Linear Mixed-Effects Models using lme4. J. Stat. Softw. 67. https://doi.org/10.18637/jss.v067.i01.

Bennet, S., McConnel, T., Trubatch, S.L., 1974. Quantitative analysis of the speed of snakes as a function of peg spacing. J. Exp. Biol. 60, 161–165.

Bergmann, P.J., 2015. Convergent evolution of body shape in squamate reptiles. In: Bininda-Edmonds, O.R.P., Powell, G.L., Jamniczky, H.A., Bauer, A.M., Theodor, J. (Eds.), All Animals Are Interesting: A Festschrift in Honour of Anthony P. Russell. BIS-Verlag, Oldenburg, Germany, pp. 245–277.

Bergmann, P.J., Irschick, D.J., 2010. Alternate pathways of body shape evolution translate into common patterns of locomotor evolution in two clades of lizards. Evolution 64, 1569–1582. https://doi.org/10.1111/j.1558-5646.2009.00935.x.

Bergmann, P.J., Irschick, D.J., 2012. Vertebral evolution and the diversification of squamate reptiles. Evolution 66, 1044–1058. https://doi.org/10.1111/j.1558-5646.2011.01491.x.

Bogert, C.M., 1947. Rectilinear locomotion in snakes. Copeia 253. https://doi.org/10.2307/1438921.

Brainerd, E.L., Patek, S.N., 1998. Vertebral column morphology, C-start curvature, and the evolution of mechanical defenses in tetraodontiform fishes. Copeia 971. https://doi.org/10.2307/1447344.

Brainerd, E.L., Baier, D.B., Gatesy, S.M., Hedrick, T.L., Metzger, K.A., Gilbert, S.L., Crisco, J.J., 2010. X-ray reconstruction of moving morphology (XROMM): precision, accuracy and applications in comparative biomechanics research. J. Exp. Zool. Part Ecol. Genet. Physiol. 313, 262–279. https://doi.org/10.1002/jez.589.

Brandley, M.C., Huelsenbeck, J.P., Wiens, J.J., 2008. Rates and patterns in the evolution of snake-like body form in squamate reptiles: Evidence for repeated re-evolution of lost digits and long-term persistence of intermediate body forms. Evolution 62, 2042–2064. https://doi.org/10.1111/j.1558-5646.2008.00430.x.

Buchholtz, E.A., 2001. Vertebral osteology and swimming style in living and fossil whales (Order: Cetacea). J. Zool. 253, 175–190. https://doi.org/10.1017/S0952836901000164.

Buchholtz, E.A., Schur, S.A., 2004. Vertebral osteology in Delphinidae (Cetacea). Zool. J. Linn. Soc. 140, 383–401. https://doi.org/10.1111/j.1096-3642.2003.00105.x.

Chen, J.J., 2006. Differential leg function in a sprawled-posture quadrupedal trotter. J. Exp. Biol. 209, 249–259. https://doi.org/10.1242/jeb.01979.

D'Août, K., Aerts, P., 1999. A kinematic comparisons of forward and backward swimming in the eel *Anguilla anguilla*. J. Exp. Biol. 202, 1511–1521.

Donley, J.M., Dickson, K.A., 2000. Swimming kinematics of juvenile kawakawa tuna (*Euthynnyus affinis*) and chub mackerel (*Scomber japaonicus*). J. Exp. Biol. 203, 3103–3116.

Fischer, M.S., Krause, C., Lilje, K.E., 2010. Evolution of chameleon locomotion, or how to become arboreal as a reptile. Zoology 113, 67–74. https://doi.org/10.1016/j.zool.2009.07.001.

Fish, F.E., 1998. Biomechanical perspective on the origin of Cetacean flukes. In: Thewissen, J.G.M. (Ed.), The Emergence of Whales: Evolutionary Patterns in the Origin of Cetacea, Advances in Vertebrate Paleobiology. Springer, Boston, MA, US, pp. 303–324. https://doi.org/10.1007/978-1-4899-0159-0_10.

Gans, C., 1962. Terrestrial locomotion without limbs. Am. Zool. 2, 167–182. https://doi.org/10.1093/icb/2.2.167.

Gans, C., 1973. Locomotion and burrowing in limbless vertebrates. Nature 242, 414–415. https://doi.org/10.1038/242414a0.

Gans, C., 1974. Biomechanics: An Approach to Vertebrate Biology. Lippincott.

Gans, C., 1975. Tetrapod limblessness: evolution and functional corollaries. Am. Zool. 15, 455–467. https://doi.org/10.1093/icb/15.2.455.

Gans, C., 1984. Slide-pushing: a transitional locomotor method of elongate squamates. Symp. Zool. Soc. Lond. 52, 13–26.

Gans, C., 1986. Locomotion of limbless vertebrates: pattern and evolution. Herpetologica 42, 33–46.

Gans, C., Gasc, J.-P., 1990. Tests on the locomotion of the elongate and limbless reptile *Ophisaurus apodus* (Sauria: Anguidae). J. Zool. 220, 517–536. https://doi.org/10.1111/j.1469-7998.1990.tb04731.x.

Gans, C., Morgan, W.K., Allen, E.S., 1992. Surface locomotion of the elongate and limbless lizard *Anniella pulchra* (Anguidae). Herpetologica 48, 246–262.

Gasc, J.-P., 1981. Axial musculature. In: Gans, C., Parsons, T.S. (Eds.), Biology of the Reptilia. Academic Press, New York, pp. 355–435.

Gasc, J.-P., Gans, C., 1990. Tests on locomotion of the elongate and limbless lizards *Anguis fragilis* (Squamata: Anguidae). Copeia 1055. https://doi.org/10.2307/1446489.

Gillis, G.B., 1996. Undulatory locomotion in elongate aquatic vertebrates: Anguilliform swimming since Sir James Gray. Am. Zool. 36, 656–665. https://doi.org/10.1093/icb/36.6.656.

Gillis, G.B., 1998. Environmental effects on undulatory locomotion in the American eel *Anguilla rostrata*: kinematics in water and on land. J. Exp. Biol. 201, 949–961.

Gliwicz, J., 1988. Sexual dimorphism in small mustelids: body diameter limitation. Oikos 53, 411. https://doi.org/10.2307/3565544.

Gomez, C., Özbudak, E.M., Wunderlich, J., Baumann, D., Lewis, J., Pourquié, O., 2008. Control of segment number in vertebrate embryos. Nature 454, 335–339. https://doi.org/10.1038/nature07020.

Gray, J., 1946. The mechanism of locomotion in snakes. J. Exp. Biol. 23, 101–120.

Greer, A.E., 1987. Limb reduction in the lizard genus *Lerista*. 1. Variation in the number of phalanges and presacral vertebrae. J. Herpetol. 21, 267. https://doi.org/10.2307/1563968.

Greer, A.E., 1990. Limb reduction in the scincid lizard genus *Lerista*. 2. Variation in the bone complements of the front and rear limbs and the number of postsacral vertebrae. J. Herpetol. 24, 142. https://doi.org/10.2307/1564221.

Hammond, G.R., Ridge, R.M.A.P., 1978. Properties of twitch motor units in snake costocutaneous muscle. J. Physiol. 276, 525–533. https://doi.org/10.1113/jphysiol.1978.sp012251.

Hedrick, T.L., 2008. Software techniques for two- and three-dimensional kinematic measurements of biological and biomimetic systems. Bioinspir. Biomim. 3, 034001. https://doi.org/10.1088/1748-3182/3/3/034001.

Hoffstetter, R., Gasc, J.-P., 1969. Vertebrae and ribs of modern reptiles. In: Gans, C. (Ed.), Ed.), Biology of the Reptili. Academic Press, New York, pp. 201–210.

Irschick, D.J., Jayne, B.C., 1998. Effects of incline on speed, acceleration, body posture and hindlimb kinematics in two species of lizard *Callisaurus draconoides* and *Uma scoparia*. J. Exp. Biol. 201, 273–287.

Irschick, D.J., Jayne, B.C., 1999. Comparative three-dimensional kinematics of the hindlimb for high-speed bipedal and quadrupedal locomotion of lizards. J. Exp. Biol. 202, 1047–1065.

Jayne, B.C., 1982. Comparative morphology of the semispinalis-spinalis muscle of snakes and correlations with locomotion and constriction. J. Morphol. 172, 83–96. https://doi.org/10.1002/jmor.1051720108.

Jayne, B.C., 1985. Swimming in constricting (*Elaphe g. guttata*) and nonconstricting (*Nerodia fasciata pictiventris*) colubrid snakes. Copeia 195. https://doi.org/10.2307/1444809.

Jayne, B.C., 1986. Kinematics of terrestrial snake locomotion. Copeia 915. https://doi.org/10.2307/1445288.

Jayne, B.C., Davis, J.D., 1991. Kinematics and performance capacity for the concertina locomotion of a snake (*Coluber constrictor*). J. Exp. Biol. 156, 539–556.

Kelley, K.C., Arnold, S.J., Gladstone, J., 1997. The effects of substrate and vertebral number on locomotion in the garter snake *Thamnophis elegans*. Funct. Ecol. 11, 189–198. https://doi.org/10.1046/j.1365-2435.1997.00077.x.

Kohlsdorf, T., Biewener, A.A., 2006. Negotiating obstacles: running kinematics of the lizard *Sceloporus malachiticus*: Obstacle crossing in lizards. J. Zool. 270, 359–371. https://doi.org/10.1111/j.1469-7998.2006.00150.x.

Kohlsdorf, T., Wagner, G.P., 2006. Evidence for the reversibility of digit loss: a phylogenetic study of limb evolution in *Bachia* (Gymnophthalmidae: Squamata). Evolution 60, 1896–1912. https://doi.org/10.1111/j.0014-3820.2006.tb00533.x.

Kuznetsova, A., Brockhoff, P.B., Christensen, R.H.B., 2017. lmerTest Package: tests in Linear Mixed Effects Models. J. Stat. Softw. 82, 1–26. https://doi.org/10.18637/jss.v082.i13.

Lande, R., 1978. Evolutionary mechanisms of limb loss in tetrapods. Evolution 32, 73–92. https://doi.org/10.1111/j.1558-5646.1978.tb01099.x.

Lauder, G.V., 1980. On the relationship of the myotome to the axial skeleton in vertebrate evolution. Paleobiology 6, 51–56. https://doi.org/10.1017/S0094837300012501.

Lenth, R., 2019. emmeans: Estimated Marginal Means, aka Least-Squares Means.

Lindell, L.E., 1994. The evolution of vertebral number and body size in snakes. Funct. Ecol. 8, 708. https://doi.org/10.2307/2390230.

Lissmann, H.W., 1950. Rectilinear locomotion in a snake (*Boa occidentalis*). J. Exp. Biol. 26, 368–379.

Long, J.H., Pabst, D.A., Shepherd, W.R., McLellan, W.A., 1997. Locomotor design of dolphin vertebral columns: bending mechanics and morphology of *Delphinus delphis*. J. Exp. Biol. 200, 65–81.

Maladen, R.D., Ding, Y., Li, C., Goldman, D.I., 2009. Undulatory swimming in sand: subsurface locomotion of the sandfish lizard. Science 325, 314–318. https://doi.org/10.1126/science.1172490.

Mehta, R.S., Ward, A.B., Alfaro, M.E., Wainwright, P.C., 2010. Elongation of the body in eels. Integr. Comp. Biol. 50, 1091–1105. https://doi.org/10.1093/icb/icq075.

Minelli, A., Fusco, G., 2004. Evo-devo perspectives on segmentation: model organisms, and beyond. Trends Ecol. Evol. 19, 423–429. https://doi.org/10.1016/j.tree.2004.06.007.

Moon, B.R., 1999. Testing an inference of function from structure: snake vertebrae do the twist. J. Morphol. 241, 217–225. https://doi.org/10.1002/(SICI)1097-4687(199909)241:3<217::AID-JMOR4>3.0.CO;2-M.

Moon, B.R., Gans, C., 1998. Kinematics, muscular activity and propulsion in gopher snakes. J. Exp. Biol. 201 (Pt. 19), 2669–2684.

Mosauer, W., 1932. On the locomotion of snakes. Sci. New Ser. 76, 583–585.

Nakagawa, S., Schielzeth, H., 2013. A general and simple method for obtaining R^2 from generalized linear mixed-effects models. Methods Ecol. Evol. 4, 133–142. https://doi.org/10.1111/j.2041-210x.2012.00261.x.

Pace, C.M., Gibb, A.C., 2011. Locomotor behavior across an environmental transition in

the ropefish, *Erpetoichthys calabaricus*. J. Exp. Biol. 214, 530–537. https://doi.org/10.1242/jeb.047902.
Parra-Olea, G., Wake, D.B., 2001. Extreme morphological and ecological homoplasy in tropical salamanders. Proc. Natl. Acad. Sci. 98, 7888–7891. https://doi.org/10.1073/pnas.131203598.
R Core Team, 2016. R: A Language and Environment for Statistical Computing. R Foundation for Statistical Computing, Vienna, Austria.
Renous, S., Gasc, J.P., 1989. Body and Vertebral Proportions in Gymnophiona (Amphibia): Diversity of Morphological Types. Copeia 837–847. https://doi.org/10.2307/1445966.
Ritter, D., 1995. Epaxial muscle function during locomotion in a lizard (*Varanus salvator*) and the proposal of a key innovation in the vertebrate axial musculoskeletal system. J. Exp. Biol. 198, 2477–2490.
Schneider, C.A., Rasband, W.S., Eliceiri, K.W., 2012. NIH Image to ImageJ: 25 years of Image Analysis. Nat. Methods 9, 671–675.
Searle, S.R., Speed, F.M., Milliken, G.A., 1980. Population marginal means in the linear model: an alternative to least squares means. Am. Stat. 34, 216–221. https://doi.org/10.1080/00031305.1980.10483031.
Sfakiotakis, M., Lane, D.M., Davies, J.B.C., 1999. Review of fish swimming modes for aquatic locomotion. IEEE J. Ocean. Eng. 24, 237–252. https://doi.org/10.1109/48.757275.
Sharpe, S.S., Ding, Y., Goldman, D.I., 2013. Environmental interaction influences muscle activation strategy during sand-swimming in the sandfish lizard *Scincus scincus*. J. Exp. Biol. 216, 260–274. https://doi.org/10.1242/jeb.070482.
Summers, A.P., O'Reilly, J.C., 1997. A comparative study of locomotion in the caecilians *Dermophis mexicanus* and *Typhlonectes natans* (Amphibia: Gymnophiona). Zool. J. Linn. Soc. 121, 65–76. https://doi.org/10.1111/j.1096-3642.1997.tb00147.x.
Swanson, B.O., Gibb, A.C., 2004. Kinematics of aquatic and terrestrial escape responses in mudskippers. J. Exp. Biol. 207, 4037–4044. https://doi.org/10.1242/jeb.01237.
Tautz, D., 2004. Segmentation. Dev. Cell 7, 301–312. https://doi.org/10.1016/j.devcel.2004.08.008.
Walter, R.M., 2003. Kinematics of 90° running turns in wild mice. J. Exp. Biol. 206, 1739–1749. https://doi.org/10.1242/jeb.00349.
Wang, J., Blackburn, T.J., 2000. The AAPM/RSNA physics tutorial for residents: X-ray image intensifiers for fluoroscopy. Radiogr. Rev. Publ. Radiol. Soc. N. Am. Inc 20, 1471–1477. https://doi.org/10.1148/radiographics.20.5.g00se181471.
Ward, A.B., Azizi, E., 2004. Convergent evolution of the head retraction escape response in elongate fishes and amphibians. Zoology 107, 205–217. https://doi.org/10.1016/j.zool.2004.04.003.
Ward, A.B., Brainerd, E.L., 2007. Evolution of axial patterning in elongate fishes. Biol. J. Linn. Soc. 90, 97–116. https://doi.org/10.1111/j.1095-8312.2007.00714.x.
Ward, A.B., Mehta, R.S., 2010. Axial elongation in fishes: Using morphological approaches to elucidate developmental mechanisms in studying body shape. Integr. Comp. Biol. 50, 1106–1119. https://doi.org/10.1093/icb/icq029.
Ward, A.B., Mehta, R.S., 2014. Differential occupation of axial morphospace. Zoology 117, 70–76. https://doi.org/10.1016/j.zool.2013.10.006.
Ward, A.B., Costa, A., Monroe, S.L., Aluck, R.J., Mehta, R.S., 2015. Locomotion in elongate fishes: A contact sport. Zoology 118, 312–319. https://doi.org/10.1016/j.zool.2015.06.002.
Wiens, J.J., Brandley, M.C., Reeder, T.W., 2006. Why does a trait evolve multiple times within a clade? Repeated evolution of snakelike body form in squamate reptiles. Evol. Int. J. Org. Evol. 60, 123–141.
Zug, G.R., 1972. Anuran Locomotion: Structure and Function. I. Preliminary Observations on Relation between Jumping and Osteometrics of Appendicular and Postaxial Skeleton. Copeia 613–624. https://doi.org/10.2307/1442720.